

新型催化材料

Novel Catalyst Materials

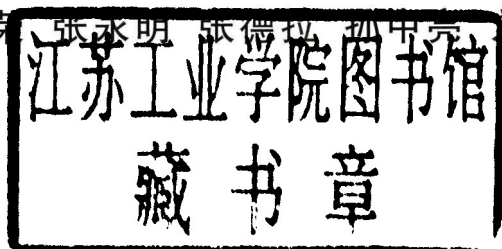
熊春荣 张永明 张德拉 孙中亮 刘钟馨 编著

海南出版社

新型催化材料

Novel Catalyst Materials

熊春荣 张永明 张德拉 孙中亮 刘钟馨 编著



海南出版社

图书在版编目 (CIP) 数据

新型催化材料: 英文 / 熊春荣等编著. Novel Catalyst Materials —海口: 海南出版社, 2009.5

ISBN 978-7-5443-3065-7

I. ①新...②N... II. 熊... III. 催化剂—原料—高等学校—教材—英文 IV. TQ426.4

中国版本图书馆 CIP 数据核字 (2009) 第 089985 号

新型催化材料 Novel Catalyst Materials

作 者: 熊春荣 张永明 张德拉 孙中亮 刘钟馨

责任编辑: 何晓玲

封面设计: 颜好强

印刷装订: 海南金永安印刷有限公司

海南出版社 出版发行

地址: 海口市金盘开发区建设三横路 2 号

邮编: 570216

电话: 0898-66830931 66830932

网址: <http://www.hncbs.cn>

E-mail: 740073619@qq.com

经销: 全国新华书店经销

开本: 787mm × 1092mm 1/16

字数: 550 千字

印张: 19.5

版次: 2009 年 5 月第 1 版 2009 年 5 月第 1 次印刷

书号: ISBN 978-7-5443-3065-7

定价: 38.00 元

Content

Part I Microporous materials and their applications.....	1
Chapter 1. Zeolite ZSM-5 and ZSM-11.....	2
Section 1. Fabrication of ZSM-5 with different silicon-to-aluminum ratios.....	3
1.1. Progress in fabrication of ZSM-5.....	3
1.2. Techniques and methods	4
1.3. Characterization and application	9
1.4. Summary	15
Section 2. Catalytic degradation of polystyrene over the modified ZSM-11 zeolite.....	17
2.1. Progress in fabrication of the modified ZSM-11 zeolite	17
2.2. Techniques and methods.....	17
2.3. Characterization and application.....	18
2.4. Summary	21
Chapter 2. Zeolite mordenite	22
Section 1. The phase transformation in the crystallization of Fe containing mordenite.....	23
1.1. Progress in the crystallization of Fe-mordenite	23
1.2. Techniques and methods	23
1.3. Characterization and properties	23
1.4. Summary.....	27
Section 2. Ethanol conversion to ethylene using metal-mordenite catalysts.....	28
2.1. Progress in ethanol conversion to ethylene.....	28
2.2. Techniques and methods.....	28
2.3. Characterization and application.....	30
2.4. Summary.....	34
Chapter 3. Zeolite Y.....	36
Section 1. The properties of the zeolite Y catalyst with different crystal sizes in FCC.....	38
1.1. Progress of the zeolite Y catalyst in FCC.....	38
1.2. Techniques and methods.....	39
1.3. Properties of the catalysts	42
1.4. Summary.....	57
Section 2. Catalysts based on Y zeolite nanoparticles for heavy oil cracking.....	58
2.1. Progress in catalysts based on Y zeolite for heavy oil cracking.....	58
2.2. Techniques and methods.....	58
2.3. Characterization and application	60
2.4. Summary	75
Chapter 4. Fabrication of nanosized ZSM-5	76
1. Progress in fabrication of nanosized ZSM-5	76
2. Techniques and methods.....	76
3. Characterization and properties.....	78
4. Summary	84
Part II Mesoporous Silicates	85
Chapter 5. An overview of mesoporous materials and mesoporous silicate materials.....	86
1. Mesoporous materials.....	86
2. Mesoporous silicate materials.....	87

Chapter 6. Review of soft-templating approach to prepare mesoporous silicates.....	90
1. Progress in templating approach to prepare mesoporous silicates.....	90
2. Synthesis mechanism and pathway.....	92
3. Synthesis of mesoporous silicate molecular sieves.....	101
4. Controllable synthesis on mesoscale.....	111
5. Morphology control.....	131
6. Summary and outlook.....	137
Part III Fabrication of nano oxides and their applications.....	140
Chapter 7. Nanomaterials and nanocatalysts.....	141
1. Nanomaterials and nanocatalysts.....	141
2. Nano-TiO ₂ catalyst for photocatalytic degradation of phenols.....	141
Chapter 8. TiO₂ Nanofibers and core-shell structures based on mesoporous templates.....	144
1. Progress in TiO ₂ nanofibers	144
2. Techniques and methods	144
3. Characterization and properties	144
4. Summary	148
Chapter 9. Fabrication of TiO₂ nanofibers from a mesoporous silica film.....	149
1. Progress in techniques for fabrication of TiO ₂ nanofibers	149
2. The techniques and methods	149
3. Characterization and properties	150
4. Summary	153
Chapter 10. Mesoporous molecular sieve derived TiO₂ nanofibers doped with SnO₂.....	154
1. Progress in TiO ₂ -SnO ₂ materials	154
2. Techniques and methods.....	154
3. Properties and application	156
4. Summary	164
Chapter 11. Fabrication of silver vanadium oxide and V₂O₅ nanowires	165
1. Progress in vanadium oxide and their application.....	165
2. Techniques and methods.....	166
3. Characterization and properties.....	166
4. Summary.....	174
Chapter 12. A novel method to prepare oxide nanomaterials.....	175
1. Progress in new methods to prepare oxide nanomaterials.....	175
2. Principle of the microwave method.....	175
3. Techniques and methods.....	176
4. Characterization and properties.....	178
5. Summary.....	179
Part IV Homogeneous and heterogeneous catalysis	180
Chapter 13. From homogeneous catalysis to heterogeneous catalysis.....	181
1. Brief history of homogeneous and heterogeneous catalysis	181
2. Homogeneous catalysis.....	181
3. Heterogeneous catalysis	184
4. Summary	190
Chapter 14. Homogeneous systems in catalytic asymmetric epoxidation	191
1. Brief History of catalytic asymmetric epoxidation.....	191
2. Homogeneous systems in catalytic asymmetric epoxidation.....	191
2.1. Sharpless systems	191

2.2. Porphyrin systems	197
2.3. Salen systems	204
2.4. BINOL systems.....	210
2.5. Chiral carbonyl compound systems	214
2.6. Chiral iminium salts	222
2.7. Other homogeneous systems	225
3. Heterogeneous systems in catalytic asymmetric epoxidation	234
3.1. Supported sharpless systems	235
3.2. Supported porphyrins systems	239
3.3. Supported salen(metal) systems	240
3.4. Phase transfer catalysis systems	255
3.5. Other heterogeneous systems	261
4. Summary	264
Chapter 15. Recent progress in zeolitic catalysts for the petroleum refining and petrochemical processing.....	266
1. Brief history of zeolite synthesis and zeolitic catalysts.....	266
2. Overview of petroleum refining and petrochemical processing catalys.....	267
3. The future promise.....	273
Part V References.....	276
Chapter 1	276
Chapter 2	276
Chapter 3	278
Chapter 4	279
Chapter 5	280
Chapter 6	281
Chapter 7	287
Chapter 8	287
Chapter 9	288
Chapter 10	288
Chapter 11	289
Chapter 12	291
Chapter 13	291
Chapter 14	292
Chapter 15	303

Part I

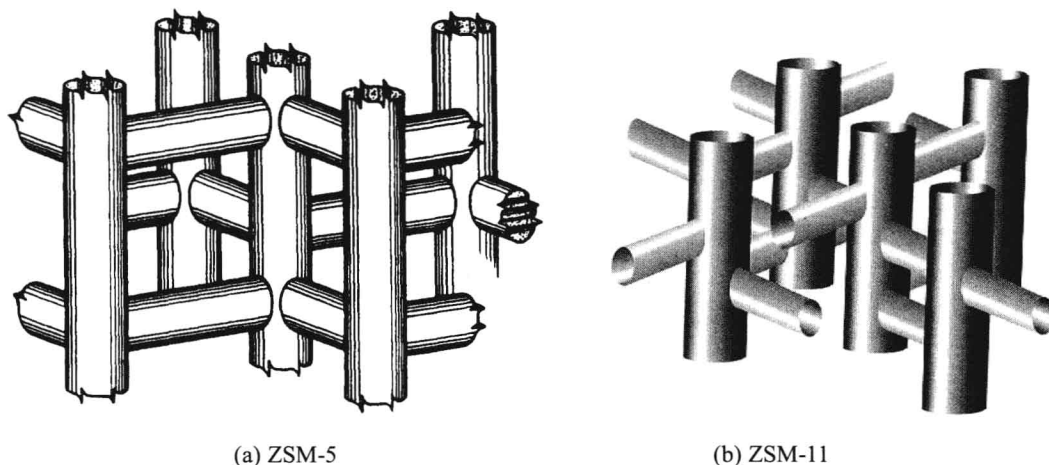
Microporous Materials and Their Applications

Microporous materials are solids containing interconnected pores with an opening size less than <2 nm. Zeolite is the most fascinating class among them with important applications in catalysis, gas separation and ion exchange due to a porous structure and a large specific surface area of typically $300\text{--}1500\text{ m}^2\cdot\text{g}^{-1}$. In the past decades, much effort has been made to optimize the porosity of these materials for different applications. It is well known that designing new microporous materials would be very important for both fundamental research and industrial applications.

This part aims to introduce the popular and important microporous materials and their applications in petrochemical process.

Chapter 1. Zeolite ZSM-5 and ZSM-11

The ZSM-5 (also known as MFI) is a zeolite with a high silica to alumina ratio. The substitution of an aluminum ion (charge 3+) for a silicon ion (charge 4+) requires the additional presence of a proton. This additional proton gives the zeolite a high level of acidity, which causes its activity. ZSM-5 is a highly porous material and throughout its structure it has an intersecting two-dimensional pore structure. ZSM-5 has two types of pores, both formed by 10-membered oxygen rings. As showed in scheme1-1(a), the ZSM-5 zeolites have a system of straight channels (pore size: 0.53×0.56 nm) interconnected by zigzag channels (pore size: 0.51×0.55 nm). This unique two-dimensional pore structure allows a molecule to move from one point in the catalyst to any where else in the particle. The large openings are the elliptical, straight pores in ZSM-5. For the MTG process it is the pores created by these 10-oxygen rings, along with the zigzag pores intersecting them, that are essential to the formation of products that are desirable components of gasoline. An 8-oxygen ring zeolite will not produce molecules with 6 or more carbons, molecules of this size will not fit into the small pores of these zeolites. The large pores of a 12-oxygen ring zeolite produce large amounts of C-11 and C-12 compounds, which are undesirable products for gasoline. ZSM-5 is mainly used for hydrocarbon interconversion, meta-xylene to para-xylene, for example. ZSM-5 and ZSM-11 are structurally similar and sometimes referred to as pentasil zeolites. The ZSM-5, ZSM-11 and their mixtures are characterized by the X-ray diffraction.



Scheme1-1. Schematics of the pore structure of ZSM-5 and ZSM-11

As showed in scheme1-1(b), the ZSM-11 (also known as MEL) zeolite pore size is similar to that for ZSM-5, but it has intersecting straight channels (pore size: 0.543×0.53 nm), that is the ZSM-11 contains a two dimensional 10-ring pore structure, both sets of pores are straight. The ZSM-11 have the potential to continuously separate mixtures by both adsorption and molecular sieving because the zeolite pores are of molecular size.

Section 1. Fabrication of ZSM-5 with Different Silicon-to-Aluminum Ratios

1.1. Progress in fabrication of ZSM-5

The works in this section is focused on the synthesis, characterization and catalytic activity of ZSM-5 zeolites having variable silicon-to-aluminum ratios^[1].

The use of alkyl lead compounds in gasoline is being discouraged worldwide. Instead, a number of oxygenates ethers are currently being blended with gasoline to produce high-octane gasoline. These include methyl tertiary butyl ether (MTBE), ethyl tertiary butyl ether (ETBE), tertiary amyl methyl ether (TAME), tertiary amyl ethyl ether (TAEE) and diisopropyl ether (DIPE). MTBE is a very attractive choice of additives in terms of economics, compatibility and performance^[2] especially in the boiling range where gasoline typically shows its lowest antiknock characteristics^[3]. The addition of MTBE not only increases the octane number but also reduces the concentration of carbon monoxide and hydrocarbons in the exhaust of vehicles. Vehicles operating on MTBE–gasoline blends can also be fitted with catalytic converters to further reduce the concentration of toxic constituents in exhaust emissions.

The commercial production of MTBE involves liquid phase electrophilic addition reactions of isobutene with methanol below 373 K over sulfonated ionexchange resins such as Amberlyst 15. Diisobutene and TBA are the major by-products formed by dimerization of isobutene, and reaction of water with isobutene, respectively. Although the performance of Amberlyst 15 is good, it has some shortcomings including thermal instability, acid leaching from the resin surface, and a high sensitivity to the methanol-to-isobutene ratio. The application of zeolite catalysts for MTBE production is attractive due to their high temperature stabilities and greater selectivities resulting from their restricted pore size. Thus, they can be utilized as environmentally favorable catalysts. A summary of studies on the use of zeolite related materials for MTBE synthesis is reported below.

The liquid phase synthesis of MTBE from methanol and isobutene over beta and USY zeolite catalysts was studied in the temperature range 30–120°C. Up to 100°C, commercial beta zeolite samples with small crystal sizes were more active than the Amberlyst 15 and noticeably more active than USY zeolite. At optimized reaction conditions, MTBE yields of 85%–90% can be reached with beta zeolite. Beta zeolite did not show any deactivation after more than 50 h on stream at 65°C, 1.4 MPa pressure, and a WHSV of 14 h⁻¹. The catalytic activity of the both zeolites was related to their external specific surface area, and to the concentration of bridging hydroxyls and silanol groups in the mesopores. A zeolite H-beta sample with a Si/Al ratio of 36 was found to have an optimum silanol and bridging hydroxyl content leading to stoichiometric methanol and isobutene adsorption, and to the highest activity and highest MTBE yields^[4].

The synthesis of MTBE from methanol and isobutene in a gas–solid heterogeneous system over sulfur-promoted zirconia catalysts has been studied in the reaction temperature range 90–110°C, and at methanol-to-isobutene molar ratios that ranged from 1.0 to 1.3. The catalyst acidity was a direct function of the sulfur load, this in turn was a consequence of the calcination temperature. The highest activity was observed on the sample calcined at 600 °C; the value was comparable with that of the reference catalyst Amberlyst 15 under the same conditions. A direct relationship between catalyst acidity and conversion was not observed. The injection of water completely poisoned the catalyst in a reversible manner^[5].

The gas phase synthesis of MTBE from methanol and isobutene has been studied using silica-supported heteropoly acids. The activity of a Dawson-type tungstophosphoric acid, H₆P₂W₁₈O₆₂/SiO₂, was comparable to that of a sulfonated polymer resin, Amberlyst 15, and its selectivity was higher. A Keggin-type heteropoly acid, H₃PW₁₂O₄₀/SiO₂, was also efficient for this reaction, while unsupported H₃PW₁₂O₄₀ was much less active than unsupported H₆P₂W₁₈O₆₂. When H₆P₂W₁₈O₆₂ was supported on SiO₂, the MTBE selectivity was increased with respect to methanol, but decreased with respect to isobutene^[6].

The gas phase synthesis of MTBE was also investigated using three types of zeolites modified by ion-exchange with ammonium fluoride, the parent materials being HY, H-mordenite, and HZSM-5. Modification of zeolites by fluoride-exchange was found to enhance the MTBE synthesis activity for all three types of zeolites without impairing their excellent selectivity. The mechanism of activity enhancement by fluoride-modification appears to be related to the formation of extra-lattice Al rather than to the presence of fluoride ions^[7].

Several studies on the synthesis of MTBE from methanol and t-butanol (TBA) have been published^[8-10]. Using microporous niobium silicate in the gas phase at temperatures in the range from 50 to 100 °C and at atmospheric pressure, good selectivity for MTBE formation was achieved at low reaction temperatures, with no catalyst deactivation during a period of more than 23 h on stream at 70°C^[8]. This reaction has also been studied using beta zeolite catalysts. Increasing the reaction temperature resulted in an increase in TBA conversion with concomitant decrease of MTBE selectivity. The TBA conversion decreased with increasing calcination temperature and more alkali metal ion-exchange of H-beta zeolite. The results were correlated with the catalyst surface area and acidity^[9].

Three classes of solid inorganic acid catalyst were demonstrated by Knifton and Edwards^[10] to be effective for MTBE syntheses from methanol/tbutanol mixtures using a continuous, plug-flow, reactor system. These catalysts include heteropoly acids, such as 12-tungstophosphoric acid and 12-molybdophosphoric acid, on groups III and IV oxide supports, such as titania, HF-treated montmorillonite clays, as well as mineral acid-activated clays. An unexpected, in situ, phase separation of the desired MTBE plus other isobutene products from aqueous methanol was observed at high conversion levels (>80%) and at operating temperatures greater than 160°C. Milder etherification conditions allow MTBE selectivity to reach 94 mol% and sustained etherification activity for the HF loaded clay catalyst even with crude TBA feedstocks.

In this section, it was presented that gas phase synthesis of MTBE from methanol and isobutene using ZSM-5 zeolites having silicon-to-aluminum molar ratios in the range 10–100. These zeolites were synthesized using a rapid crystallization method utilizing a temperature programmed templating procedure. A number of different characterization techniques were used for elucidation of compositional and other characteristics of the synthesized zeolites.

1.2. Techniques and methods

1.2.1. Synthesis of MFI zeolites

1.2.1.1 Experimental set-up: A high-pressure autoclave (manufactured by Parr Instrument Company, Moline, Illinois, USA) was employed for the rapid crystallization of zeolites (Fig. 1-1).

The reactor consisted of one-liter 316 stainless steel cylindrical pressure vessel, reactor head, heater, and temperature and stirrer speed controllers. It was fitted with both pressure and temperature indicators. The reactor was provided with a safety rupture disk having a bursting capacity of 3008 psi.

1.2.1.2 Synthetic procedure

The following high purity reagents were used for the synthesis of zeolites: sodium metasilicate pentahydrate ($\text{Na}_2\text{SiO}_3 \cdot 5\text{H}_2\text{O}$), sodium hydroxide, sodium chloride, aluminum sulfate hexadecahydrate, concentrated sulfuric acid, and tetrapropylammonium bromide. These chemicals were obtained from Fluka. Zeolite gels having silicon-to-aluminum molar ratios ranging from 9 to 100 were prepared by altering the aluminum content of the synthesis precursors. Three solutions were prepared separately. Solution A was prepared by dissolving aluminum sulfate hexadecahydrate (0.2–15.0 g) in distilled water (60 g) containing tetrapropylammonium bromide (6.0 g) and sodium chloride (5.0 g). Solution B was obtained by dissolving the sodium metasilicate pentahydrate (100 g) in distilled water (100 g) at 343 K. Solution C consisted of tetrapropylammonium bromide (2.16 g), sodium hydroxide (2.39 g) and sodium chloride (47.5 g) dissolved in 200 g of distilled water. Solutions A and B were mixed together, and then solution C was added with vigorous stirring. Gelation took place. The gel obtained was stirred for 5 min and

then the pH was adjusted to 10.0 by careful dropwise addition of concentrated sulfuric acid. The gel was stirred vigorously for 80 min to homogenize it. This was then allowed to age overnight under stirring at 1000 rpm. The pH of the gel was finally adjusted to 10.0 ± 0.1 and charged into the reactor vessel, which was heated in a temperature programmed mode. Rapid crystallization was achieved by heating the gel with constant stirring at a rate of $2\text{ }^{\circ}\text{C min}^{-1}$ up to 433 K and subsequently at $10\text{ }^{\circ}\text{C min}^{-1}$ up to 483 K. The heating was regulated at this temperature overnight. The contents of the reactor vessel were then allowed to cool to ambient temperature. They were then mixed with an equal volume of distilled water and stirred for 1 h to wash out impurities and extraneous ions from the zeolite pores and particles. The contents were then filtered through Whatman ashless filter paper No 4 and washed several times until the washing was neutral. The crystals finally obtained were dried overnight at 393 K. The zeolite obtained after drying was designated as as-synthesized (ZAS).

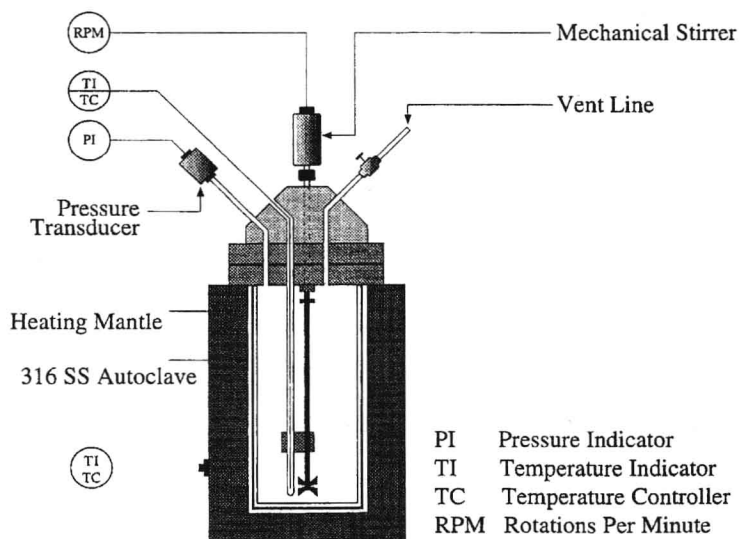


Fig.1-1. Diagram of the autoclave used for rapid crystallization of MFI zeolites.

1.2.2. Pretreatment of MFI zeolites

Calcination of zeolites was performed in order to remove the template from the as-synthesized zeolites, and to eliminate ammonia after ion-exchange with ammonium nitrate solution. The zeolites were calcined at 873 K for 3 h in $100\text{ cm}^3\text{ min}^{-1}$ of air flow. The temperature of the furnace was programmed at $10\text{ }^{\circ}\text{C min}^{-1}$. After the first calcination, the zeolite samples were termed as calcined (ZC). These were ion-exchanged to replace sodium ions for hydrogen ions present on the active sites. A 1.0 M aqueous solution of ammonium nitrate was used at 353 K for carrying out ion-exchange, the catalyst-to-solution ratio was 1g to 150 cm^3 and the stirring was carried out for 1 h. After ion-exchange, the zeolite was filtered, washed, and dried at 393 K overnight and then calcined at 873 K for 3 h in air flow to decompose the ammonium ions to produce hydrogen form (ZCIC).

1.2.3. Characterization of zeolites

The MFI zeolites prepared were characterized for their chemical composition, crystallinity, thermal behavior, and morphology. The determination of aluminum and silicon contents in zeolite samples was carried out using standard inductively coupled plasma (ICP) method. The samples for ICP analysis were prepared by fusing the zeolite with sodium hydroxide. Sodium contents were determined using a Dr. Lange Flame Photometer which had been calibrated with standard sodium chloride solutions. Thermal analyses were carried out using a Simultaneous Thermal Analyzer Model STA 429, manufactured by Netzsch, which performed thermogravimetry and differential

thermal analysis simultaneously. A preweighed zeolite sample of 100 mg that was ground to 125 mesh size was used, along with the same weight of pre-calcined ultrex grade aluminum oxide as a reference sample. The temperature of the sample was raised at a uniform rate of 10 °C min⁻¹ from ambient to 1423 K in an air flow at a rate of 100 cm³ min⁻¹. In the thermograms, the weight loss, the differential temperature, and the temperature of the sample were plotted simultaneously. The FT-IR spectra were recorded using Perkin-Elmer Model 1600 Infrared Spectrophotometer in the range 4000–400 cm⁻¹ on thin wafers of KBr in which 1% (w/w) of zeolite was dispersed. Crystallinity was checked using a JEOL JDX-3530 X-ray diffractometer equipped with a Cu fine focus X-ray tube working at a generator potential of 40 kV and a generator current of 30 mA with divergence and scatter slit set at 1°, receiving slit at 0.2 mm, and a nickel filter. Scanning was continuous and the scanning speed and interval of data collection was 0.01° (2θ)s⁻¹ and the angles scanned were from 4 to 50° (2θ). The zeolite samples were also characterized by scanning electron microscopy using a JEOL scanning microscope model JSM-T330. The samples in the powdered form were dried at 453 K overnight and then mounted on aluminum disks. In this process, a thin layer of sample powder was spread and deposited on each aluminum disk having carbon pads. These samples were then evacuated at 1.3 Pa vacuum for 2 h using an Edwards freeze dryer, and then immediately coated with gold. Coating was performed for 6 min at 610 Pa in an Edwards sputter coater. The gold coated disks were then mounted in the sample holder of the instrument and the data was collected over the range of 5000–20,000 magnification power. Surface area and pore structure were measured using fully automated ASAP 2000 equipment (Micromeritics, USA). The zeolite samples were heated overnight in an oven at 473 K in order to remove moisture. A weighed quantity of dry zeolite sample was degassed overnight at 573 K under a vacuum of 3 μmHg. The sample was allowed to cool, reweighed and connected to the analysis port as quickly as possible in order to avoid any readsorption of moisture. At the analysis port, nitrogen was fed into the tube and adsorption of the gas took place. This was followed by desorption of nitrogen and then calculation of the surface area and other parameters.

1.2.4. Catalytic evaluation of synthesized zeolites

1.2.4.1. Experimental set-up

The packed-bed reaction system used for screening of MFI zeolite catalysts for MTBE synthesis is shown in Fig. 1-2. Experiments were carried out at atmospheric pressure in a fixed bed tubular stainless steel reactor. The feed section was designed to supply the feed to the reaction system under controlled pressure and flow rate and consisted of a methanol storage tank, a methanol feed pump, air, nitrogen and isobutene gas cylinders, and a Brook's mass flow meter. The feed tank was equipped with pressure indicators, filling port and a side Teflon tube to show the liquid level inside the tank. Methanol liquid was fed to the unit by a Milton Roy Minipump (Model 396-57). Isobutene gas from the cylinder was supplied at a regulated flow using a mass flow meter (Brooks Model 5850C). The isobutene gas was mixed with methanol before the preheating zone. The different feeds were delivered to the reaction system through 10 mm o.d. stainless steel tubing. The preheater was made of 10 mm o.d. stainless steel coiled tubes insulated with a high heat-resistant heating tape to preheat the feed and to maintain stable temperature during the operation.

The reactor used was a 380 mm long stainless steel tube having 9.0 mm i.d. and 1.0 mm thickness. The reactor was housed in a three-zone furnace; the temperatures of the reactor were measured at the inlet, center and outlet of the reactor. The reactor was fitted with a mesh screen at the inlet, to distribute the feed mixture uniformly across the reactor radius. The heating rate and the temperature were maintained by a temperature controller. The product collection section was designed to separate and collect the reaction products into liquid and gaseous fractions. It consisted of a two stage cooling system supplied by Brinkman Instrument Co., USA. A mixture of ethylene glycol and water was used as the circulating medium. Condensed products were collected at sampling times through a down-flow drain valve located at the bottom of the product collector

which was maintained at 263 K. Detailed reaction parameters to produce MTBE from methanol and isobutene are given in Table 1-1.

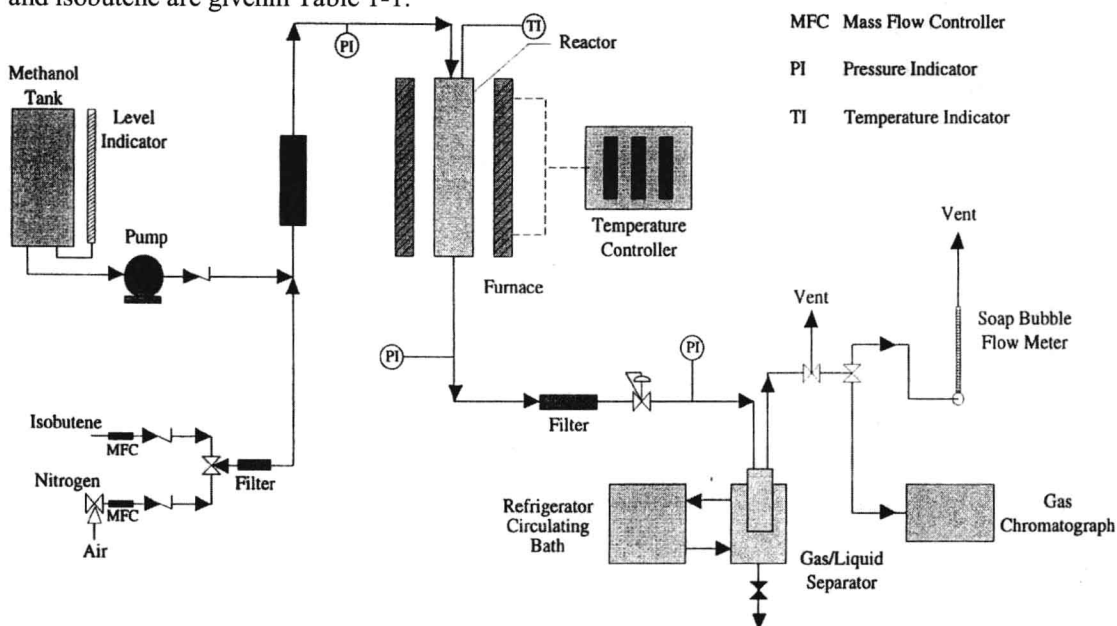


Fig.1-2. Diagram of the packed-bed reaction system used for catalytic evaluation of MFI zeolite catalysts.

Table 1-1 Packed-bed reaction parameters to produce MTBE from methanol and isobutene

Parameters	Values
Catalyst pellet size (mm)	1–2
Isobutene flow (mol h ⁻¹)	11.6×10^{-2} (6.51)
Methanol flow (mol h ⁻¹)	23.4×10^{-2} (7.49)
Total reactant flow (mol h ⁻¹)	35.0×10^{-2} (14.0)
WHSV	2.0
Methanol-to-isobutene molar ratio	2.0
Reaction temperature (K)	343, 353, 363 and 373
Reactor dimensions (mm)	Tubular stainless steel; 380 length \times 9.0 i.d.

Values shown in the parentheses are measured in g h⁻¹.

1.2.4.2. Reaction procedure

The ion-exchanged calcined zeolite powder was converted into 1–2 mm size pellets needed for catalytic reactions. For this purpose, the zeolite powder was placed in a special die and a pressure of 15,000 psi (103 MPa) was applied to produce a disk of about 2 mm thickness. This zeolite disk was broken on a sieve to produce 1–2 mm size pellets. Prior to packing the zeolite catalyst into the reactor, the bulk density of the pellets was determined by weighing a known volume of the catalyst in a 10 cm³ graduated cylinder. For all catalytic runs, 7 g of zeolite catalysts was packed in the reactor. The catalyst was placed in the center of the reactor between layers of glass wool. The bottom of the reactor contained some glass beads between the catalyst bed and the silica wool. The reactor was then mounted in position on the three-zone electric furnace enclosing the reactor.

The zeolite catalyst was calcined *in situ* at 773 K for 3 h in an air stream having a flow of 100 cm³ min⁻¹ to purge water and other volatile impurities within the zeolite pores. The calcination involved stepwise heating of the sample from ambient temperature to 773 K. The temperature was raised at a rate of 10°C min⁻¹ from ambient to 423 K this was then maintained for 20 min. The temperature was then raised to 573 K and then 673 K at the same rate; it was maintained for 20 min at each stage. Finally, the temperature was raised to 773 K, and maintained for 3 h. Following

the in situ calcination, the reactor was allowed to cool. When the temperature reached 473 K, the air flow was replaced by a nitrogen flow to purge the residual calcination products from the catalyst bed. The nitrogen flow was maintained overnight at $100 \text{ cm}^3 \text{ min}^{-1}$.

Table 1-2 Elemental composition of ZAS zeolites, and unit cell composition of ZAS, ZC and ZCIC forms of zeolites

Zeolite	Silicon (wt.%)	Aluminum (wt.%)	Sodium (wt.%)	Water (wt.%)	TPAOH (wt.%)
ZSA-10	38.7	3.81	3.11	6.2	5.4
ZSA-15	39.2	2.62	2.05	4.7	6.2
ZSA-20	41.8	2.07	1.62	4.5	6.7
ZSA-25	41.9	1.67	1.30	3.7	7.4
ZSA-50	42.3	0.82	0.63	3.2	8.2
ZSA-75	42.5	0.55	0.41	2.9	9.7
ZSA-100	42.6	0.41	0.30	2.5	10.7
Unit cell composition					
ZSA-10	$\text{Na}_{8.81}[\text{Al}_{8.90}\text{Si}_{87.1}\text{O}_{192}] \cdot (\text{H}_2\text{O})_{20.5} \cdot (\text{TPAOH})_{1.6}$				
ZSA-15	$\text{Na}_{6.19}[\text{Al}_{6.24}\text{Si}_{89.8}\text{O}_{192}] \cdot (\text{H}_2\text{O})_{18.9} \cdot (\text{TPAOH})_{2.0}$				
ZSA-20	$\text{Na}_{4.61}[\text{Al}_{4.69}\text{Si}_{91.3}\text{O}_{192}] \cdot (\text{H}_2\text{O})_{17.8} \cdot (\text{TPAOH})_{2.1}$				
ZSA-25	$\text{Na}_{3.79}[\text{Al}_{3.84}\text{Si}_{92.2}\text{O}_{192}] \cdot (\text{H}_2\text{O})_{14.5} \cdot (\text{TPAOH})_{2.3}$				
ZSA-50	$\text{Na}_{1.85}[\text{Al}_{1.90}\text{Si}_{94.1}\text{O}_{192}] \cdot (\text{H}_2\text{O})_{13.1} \cdot (\text{TPAOH})_{2.6}$				
ZSA-75	$\text{Na}_{1.20}[\text{Al}_{1.29}\text{Si}_{94.7}\text{O}_{192}] \cdot (\text{H}_2\text{O})_{12.5} \cdot (\text{TPAOH})_{3.1}$				
ZSA-100	$\text{Na}_{0.88}[\text{Al}_{0.96}\text{Si}_{95.0}\text{O}_{192}] \cdot (\text{H}_2\text{O})_{11.2} \cdot (\text{TPAOH})_{3.5}$				
ZC-10	$\text{Na}_{8.81}[\text{Al}_{8.90}\text{Si}_{87.1}\text{O}_{192}] \cdot (\text{H}_2\text{O})_{20.5}$				
ZC-15	$\text{Na}_{6.19}[\text{Al}_{6.24}\text{Si}_{89.8}\text{O}_{192}] \cdot (\text{H}_2\text{O})_{18.9}$				
ZC-20	$\text{Na}_{4.61}[\text{Al}_{4.69}\text{Si}_{91.3}\text{O}_{192}] \cdot (\text{H}_2\text{O})_{17.8}$				
ZC-25	$\text{Na}_{3.79}[\text{Al}_{3.84}\text{Si}_{92.2}\text{O}_{192}] \cdot (\text{H}_2\text{O})_{14.5}$				
ZC-50	$\text{Na}_{1.85}[\text{Al}_{1.90}\text{Si}_{94.1}\text{O}_{192}] \cdot (\text{H}_2\text{O})_{13.1}$				
ZC-75	$\text{Na}_{1.20}[\text{Al}_{1.29}\text{Si}_{94.7}\text{O}_{192}] \cdot (\text{H}_2\text{O})_{12.5}$				
ZC-100	$\text{Na}_{0.88}[\text{Al}_{0.96}\text{Si}_{95.0}\text{O}_{192}] \cdot (\text{H}_2\text{O})_{11.2}$				
ZCIC-10	$\text{H}_{8.88}\text{Na}_{0.02}[\text{Al}_{8.90}\text{Si}_{87.1}\text{O}_{192}] \cdot (\text{H}_2\text{O})_{20.5}$				
ZCIC-15	$\text{H}_{6.21}\text{Na}_{0.02}[\text{Al}_{6.24}\text{Si}_{89.8}\text{O}_{192}] \cdot (\text{H}_2\text{O})_{18.9}$				
ZCIC-20	$\text{H}_{4.67}\text{Na}_{0.02}[\text{Al}_{4.69}\text{Si}_{91.3}\text{O}_{192}] \cdot (\text{H}_2\text{O})_{17.8}$				
ZCIC-25	$\text{H}_{3.83}\text{Na}_{0.01}[\text{Al}_{3.84}\text{Si}_{92.2}\text{O}_{192}] \cdot (\text{H}_2\text{O})_{14.5}$				
ZCIC-50	$\text{H}_{1.89}\text{Na}_{0.01}[\text{Al}_{1.90}\text{Si}_{94.1}\text{O}_{192}] \cdot (\text{H}_2\text{O})_{13.1}$				
ZCIC-75	$\text{H}_{1.27}\text{Na}_{0.02}[\text{Al}_{1.29}\text{Si}_{94.7}\text{O}_{192}] \cdot (\text{H}_2\text{O})_{12.5}$				
ZCIC-100	$\text{H}_{0.94}\text{Na}_{0.02}[\text{Al}_{0.96}\text{Si}_{95.0}\text{O}_{192}] \cdot (\text{H}_2\text{O})_{11.2}$				

The reactor was allowed to cool down to the reaction temperature. After the reactor reached the desired reaction temperature, the preheater heating and product collector cooling were started and allowed to reach their equilibrium temperature. The temperature of the preheater was the same as that of the reactor, while the product collector was set at 263 K. The methanol pump was started and the different sections of the reaction system were then closely monitored until methanol reached the catalyst bed and then collected at the product collection section. At this moment, the flow rate of methanol was measured. Then, the isobutene flow was started and the methanol–isobutene mixture was preheated to the required reaction temperature and fed into the

reactor. The reaction temperature was monitored by a thermocouple located at the center of the catalyst bed. The reaction was carried out at atmospheric pressure (gas phase) and the reaction products were collected after the system reached the steady state. A methanol-to-isobutene ratio of 2:1 was used to avoid the formation of diisobutene by the dimerization of isobutene. The methanol and isobutene flow rates were 0.234 mol h^{-1} (7.5 g h^{-1}) and 0.116 mol h^{-1} (6.5 g h^{-1}), respectively, and the total reactants flow was 0.35 mol h^{-1} (14.0 g h^{-1}). The weight hour space velocity was kept at 2.0 and the methanol-to-isobutene molar ratio was 2.0. All catalysts were evaluated at temperatures of 343, 353, 363 and 373 K. The products of the reaction were collected on an hourly basis.

Table1-2 shows elemental analysis results for the zeolites ZAS-10 to ZAS-100 in terms of silicon, aluminum and sodium contents together with approximate water and TPAOH contents obtained from thermal analysis. Table1-2 also demonstrates the unit cell composition of the as-synthesized, calcined and ion-exchanged calcined zeolites calculated from the elemental analysis data. These data illustrate very clearly that as the Si/Al molar ratio increases for ZAS zeolites, the sodium and water contents decrease while the TPAOH content increases. Following calcination and replacement of sodium ions with hydrogen ions to produce the acid forms of the zeolites, the sodium contents of the zeolites (ZCIC form) were found to be in the range 5.0×10.3 to $7.0 \times 10.3 \text{ wt.}\%$, indicating a negligible sodium ion content.

Table1-3 Approximate weight percent losses obtained for as-synthesized zeolites using thermal analysis

Zeolite type	Total loss (293–873 K)	Loss of water (293–573 K)	Loss of template (573–873 K)
ZSA-10	11.6	6.2	5.4
ZSA-15	10.9	4.7	6.2
ZSA-20	11.2	4.5	6.7
ZSA-25	11.1	3.7	7.4
ZSA-50	11.4	3.2	8.2
ZSA-75	12.6	2.9	9.7
ZSA-100	13.2	2.5	10.7

The reaction products were collected from the separator in chilled glass vials and were analyzed using an HP 5890 gas chromatograph equipped with a flame ionization detector on a HP Ultra-1 capillary column, $50 \text{ m} \times 0.32 \text{ mm} \times 0.52 \mu\text{m}$ film thickness using helium as a carrier gas and the split ratio was 100:1. The detector and injector were maintained at 523 and 573 K, respectively. During the analysis, the column was maintained at 303 K isothermally. The flow rates of air, hydrogen and helium were 400, 30 and $1.4 \text{ cm}^3 \text{ min}^{-1}$, respectively. The injection volume was $0.2 \mu\text{l}$. The components of the reaction products were analyzed using diisopropyl ether as an internal standard. Percent isobutene conversion was calculated using the following formula:

$$\% \text{ isobutene conversion} = \frac{\text{isobutene in the feed} - \text{isobutene in the product}}{\text{isobutene in the feed}} \times 100$$

1.3. Characterization and application

1.3.1. Characterization of synthesized zeolites

1.3.1.1. Zeolite composition

The total percent weight losses in the temperature range 293–873 K represent water loss as well as loss of template. These two losses are overlapped in the thermogram and thus provide an approximate estimation. Weight loss in the temperature range 293–573 K represented by a broad band in the thermogram is believed to be due to water loss and was found decreasing with increasing Si/Al ratio of the zeolites (Fig. 1-4). This is because the acidity of the zeolite decreases with increasing Si/Al ratio, thus increasing its hydrophobic nature.

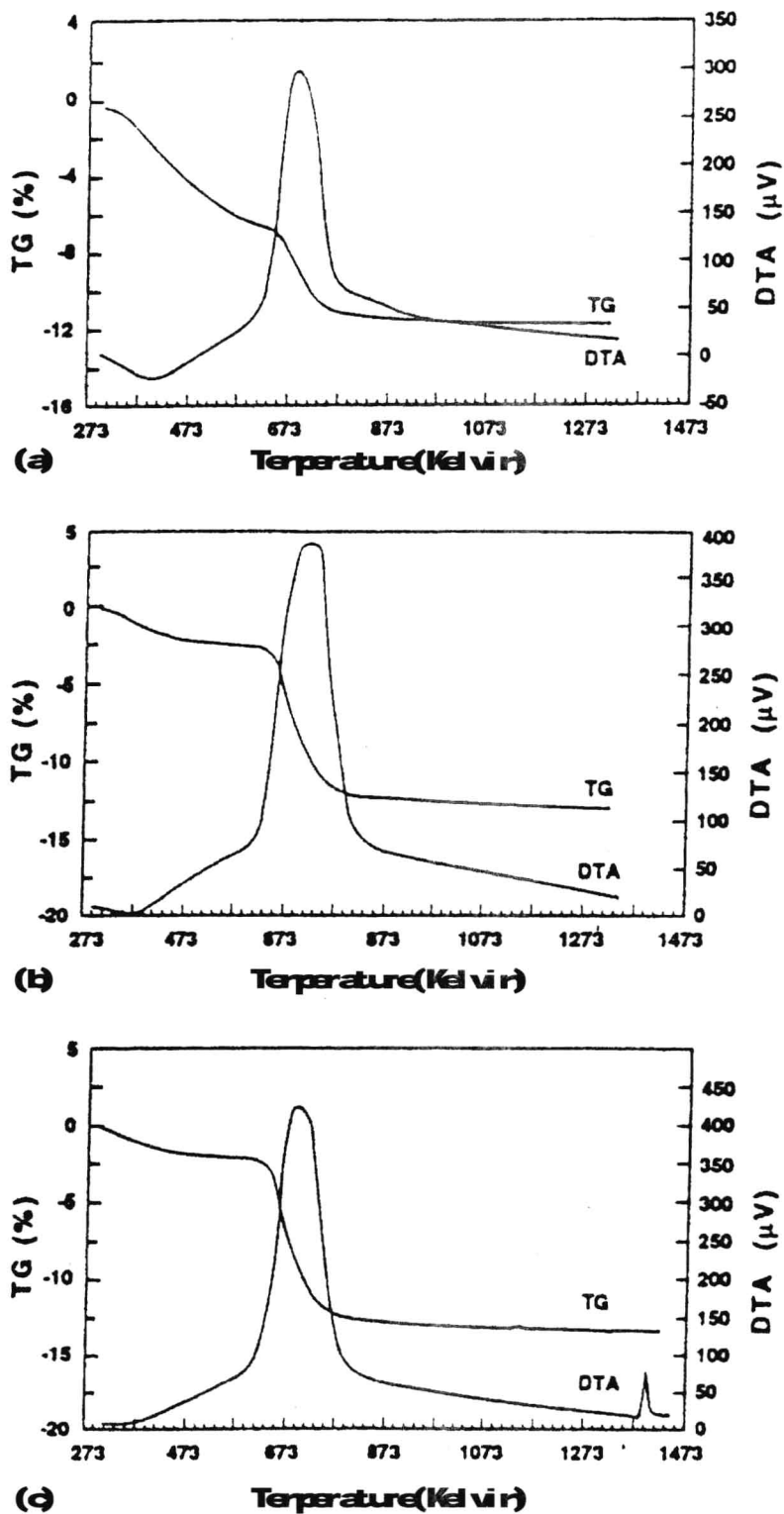


Fig.1-3 Thermograms of as-synthesized zeolites having Si/Al molar ratios of (a) 10, (b) 75 and (c) 100.

Therefore, less water is present in the zeolites with low aluminum content. The weight losses

caused by the thermolysis of template in the temperature range 573–873 K show a sharp peak in the thermogram and increase with increasing Si/Al ratio of the zeolites.

1.3.1.2. Thermal analysis

Thermal analysis was carried out to determine the thermal stability of the synthesized zeolites and to measure water and template loss. Thermograms of three representative examples are illustrated in Fig. 1-3 and data for zeolite ZAS-10 to ZAS-100 are summarized in Table 1-3. The observed exotherms are due to the oxidative decomposition of the template present in the zeolite pores. Endotherms representing water loss are overshadowed by the exotherms due to combustion of the template.

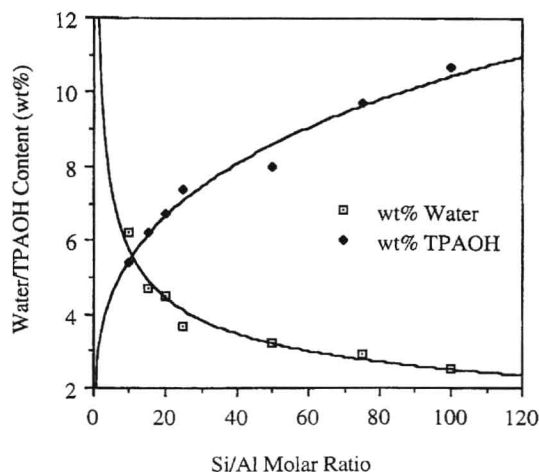


Fig.1-4 Water and TPAOH contents as a function of Si/Al molar ratio of the as-synthesized zeolites.

1.3.1.3. Fourier transform infrared spectroscopy

The FT-IR spectra of the synthesized zeolites were recorded in the range 4000–400 cm^{-1} . Fig.1-5 shows the infrared spectra of zeolite ZCIC-10 and precursor forms which are as-synthesized, calcined, ion-exchanged and calcined after ion-exchanging. These spectra show the appearance and disappearance of different absorption bands during the pretreatment procedure.

The spectra of as-synthesized zeolites ZAS-10 to ZAS-100 show weak C–H stretching absorption bands in the region 2980–2880 cm^{-1} due to presence of the template together with two broad bands at 3670 and 3460 cm^{-1} assigned to tetraalkyl ammonium O–H stretching modes. Calcination results in disappearance of absorption bands assigned to the template. Following ion-exchange with aqueous solution of ammonium nitrate, new bands appeared at 3170 and 1400 cm^{-1} due to N–H stretching and bending modes. When the ammoniated zeolite was calcined to produce the hydrogen form of the zeolite, the bands at 3170 and 1400 cm^{-1} disappeared and the intensities of O–H stretching bands increased.

Table 1-4 summarizes infrared absorption data for the ZAS zeolites in the range of 1500–400 cm^{-1} . Bands around 791, 1080 and 1219 cm^{-1} are characteristic of SiO_4 tetrahedron units^[12] and the data shows that the asymmetric stretching vibration frequencies at 1219 and 1080 cm^{-1} generally shift to higher wavenumbers with an increase in the Si/Al ratio. The absorptions at 1219 and 542 cm^{-1} provide information on the differences between these zeolites and other zeolite types. The external symmetric stretching vibration near 1219 cm^{-1} is due to the presence of structures containing four chains of five-membered rings arranged around a two-fold screw axis, as in the case of ZSM-5 structure^[13]. The absorption band around 1080 cm^{-1} is attributed to the internal asymmetric stretching vibration of Si–O–T linkage and is observed to shift towards higher wavenumbers with increasing Si/Al ratio of the zeolite.